(Received 12 November 2023, Accepted 29 December 2023, Scheduled 8 February 2024)

Ultrawideband Polarization Conversion Metasurface with Wide Incidence Angle Suitable to Reduce RCS of Planar and Curved Surfaces

Jinrong Su[1,*], Yanliang Guo[1], Haipeng Dou[2], and Xinwei Chen[1]

[1] School of Physics and Electronic Engineering, Shanxi University, Shanxi 030006, China
[2] School of Information Engineering, Shanxi Vocational University of Engineering Science and Technology, Jinzhong, China

ABSTRACT: In this paper, an ultra-wideband linear cross polarization converter based on metasurface (MS) with wide incidence angle is presented and applied to the reduction of radar cross section (RCS) for planar and conformal surfaces. A pair of bow-and-arrow shaped split ring cells is printed on an FR4 dielectric substrate. The simulated and experimental results indicate that the converter achieves a cross polarization conversion ratio (PCR) of over 90% in 11.5–28.5 GHz (85% relative bandwidth) and that its oblique incidence performance can be stabilized at $\pm 40^\circ$ with a very small loss of bandwidth (1.65%). Then, the polarization conversion metasurface (PCM) cells and their mirror cells are laid out in a checkerboard array and applied to reduce the RCS of planar and conformal surfaces. The planar PCM achieves more than 7 dB of RCS reduction in 11.4 to 29.6 GHz (88.8% relative bandwidth), and the conformal array with a center angle of 90° obtains more than 10 dB RCS reduction in 18.2 to 23.7 GHz. Due to its excellent performances, the proposed metasurface offers promising options for polarization control devices and stealth technology in Ku- and K-bands.

1. INTRODUCTION

Polarization converters are important to modern wireless communication systems. They are widely used in satellite communications, aerospace, and RCS reduction [1]. The polarization conversion of electromagnetic (EM) waves can be realized by conventional techniques, such as using the birefringence effect, liquid crystals, and Faraday effect [2, 3]. However, these techniques suffer from drawbacks of complex design process, narrow bandwidth, and large thickness, which limit their practical application.

Fortunately, the emergence of metasurface (MS) brings new hope for the development of polarization converter [4]. Utilizing powerful ability of MS to manipulate EM, people proposed various MSs to achieve polarization conversion, including frequency selective surfaces (FSS) [5–9], tunable polarization converters [10–14], chiral geometry, and anisotropic MS [15–23]. Among them, the anisotropic properties of MS are widely used in the design of reflective polarization converters, such as "double-V" [21], "grating" [22], and "split-ring" [23] MSs. However, the limited bandwidth hinders their practical application and has yet to be expanded further.

It is worth noting that the stability to oblique incidence of EM waves is also an important property of the polarization converter, which determines whether it can be used in special scenarios and curved structures. Columnar or curved surfaces are widely used in practical wireless communication applications including radomes, aircraft, ships, missiles, and various transmitters [3]. In such application scenarios, the incident angle of EM waves varies with center angle of the conformal surface, and the scattering characteristics of the PCM also depend heavily on the curvature of the conformal surface. Only converters with angular stability can satisfy these applications. To obtain this performance, an ultrathin substrate was used in [24], and the PCRs were stable when the incident angle varied from 0° to 45°. However, reducing the dielectric substrate thickness easily leads to the loss of bandwidth. To expand the bandwidth, a concentric double square ring resonator-based unit cell was designed to generate multiple plasmon resonances in [3]. An air layer was added between the grounded plane and the substrate to further increase the bandwidth. When the incident angular varies from 0° to 35° PCR is higher than 80% with relative bandwidth of 106%. However, the sandwiched air layer complicates processing and assembling. Therefore, perfect trade-off among angular stability, polarization conversion bandwidth, and structural complexity remains a challenge.

PCM can also be applied to reduce RCS in antennas and curved/straight planes [25]. The principle of PCM-based RCS reduction is phase cancellation, which is caused by the 180° phase difference of the reflected field between the cells. PCM arrays arranged in a checkerboard pattern to reduce RCS of planar surfaces is common [26–28]. For example, an ultrawideband PCM with the PCR of higher than 90% was proposed and applied to RCS reduction of planar surface in [28]. 4.8 dB RCS reduction in 10.5–35.1 GHz is achieved. As mentioned above, in many practical applications, the RCS reduction of curved surfaces is required. However, the studying fruit in this is not plentiful and substantial to meet the demands of practical applications. The sandwich structure PCM in [23] has also been used for RCS reduction of curved cylindrical surfaces. The re-

* Corresponding author: Jinrong Su (sujinrong@sxu.edu.cn).

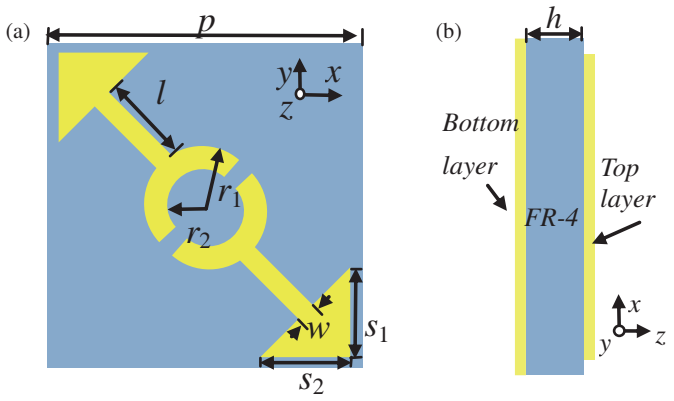

FIGURE 1. Scheme of the proposed MS unit cell: (a) Top view and (b) Side view.

TABLE 1. Design parameters of the proposed unit cell.

parameters	p	w	l	r_1	r_2	s_1	s_2	h
value/mm	6	0.4	1.5	1.2	0.8	1.8	1.8	1.6

sults showed that 10 dB RCS reduction of surface with 90° center angle at relative bandwidth of 42% was realized. As the only instance of curved surface RCS reduction using PCM, it is of pioneering significance. However, the sandwich structure is not compact enough, and curved surface RCS reduction is in great demand. Therefore, more research needs to be carried out.

This paper aims at presenting an ultra-wideband polarization converter with oblique incidence stability and high PCR, and then apply it to reduce RCS of planar and curved surfaces. A pair of bow-and-arrow shaped split ring (BASR) unit cells is designed to generate multiple resonances and thus results in an ultra-wideband of 11.5–28.5 GHz with PCR of higher than 90%. When the incident angle varies in the range of 0° to ±40°, the PCR remains higher than 85%. Also, based on the principle of phase cancellation, the PCM units and their mirror units are arranged into a checkerboard array, and broadband RCS reduction is achieved on planar and conformal surfaces. The proposed metasurface is suitable for Ku- and K-band wireless communication systems.

The paper is structured as follows. Section 2 gives the specific design and operating mechanism of the polarization converter. Section 3 addresses the application of the designed PCM to reduce RCS of both planar and curved surfaces. Section 4 gives the measured results of the PCM-based polarization converter, and Section 5 summarizes the full paper.

2. DESIGN AND PRINCIPLE

2.1. Polarization Converter Design

The proposed polarization converter unit cell consists of a pair of oppositely placed bow-and-arrow shaped split ring (BASR), a dielectric substrate, and a grounded plate, as depicted in Fig. 1. According to the reflection theory of EM waves on the interface of conductors, to generate orthotropic wave for x- or y-polarized incident wave, the resonator structure should be asymmetric about x- and y-axes and symmetric about 45° direction [17]. Thus, the BASRs are placed along the diagonal. The structures are printed on the top of FR-4 (loss angle tangent = 0.025 relative permittivity = 4.3). The optimized geometrical parameters are listed in Table 1.

CST Microwave Studio software is used to perform the numerical simulations. Due to the anisotropy of the PCM, the reflected wave of the incident EM wave consists of a co-polarized reflected component and a cross-polarized reflected component. They are equal to:

$$|R_{yy}| = |E_{yr}| / |E_{yi}| \quad (1)$$

$$|R_{xy}| = |E_{xr}| / |E_{yi}| \quad (2)$$

where x and y represent the polarization direction of the EM wave. $|R_{yy}|$ and $|R_{xy}|$ are the co-polarization reflection coefficient and cross-polarization reflection coefficient, respectively. The simulated $|R_{yy}|$ and $|R_{xy}|$ are shown in Fig. 2. One can observe that $|R_{xy}|$ is larger than -5 dB in most of the range of 11.5–28.5 GHz, while $|R_{yy}|$ is smaller than -16.5 dB. The results indicate that almost all incident waves are converted into the cross-polarization.

To further verify performance of the polarization converter, the polarization rotation angle γ and ellipticity angle β are calculated using the Stokes method [29]. First, the phase difference δ between R_{xy} and R_{yy} is calculated as:

$$\delta = \varphi_{xy} - \varphi_{yy} \quad (3)$$

When y-polarized wave is incident normally, γ and β can be obtained by:

$$\tan 2\gamma = S_2/S_1 \quad (4)$$

$$\tan 2\beta = S_3/S_0. \quad (5)$$

where $S \sim S_3$ are calculated from the Stokes formulas:

$$S_0 = T_{yy}^2 + T_{xy}^2 \quad (6)$$

$$S_1 = T_{yy}^2 - T_{xy}^2 \quad (7)$$

$$S_2 = 2T_{yy}T_{xy}\cos\delta \quad (8)$$

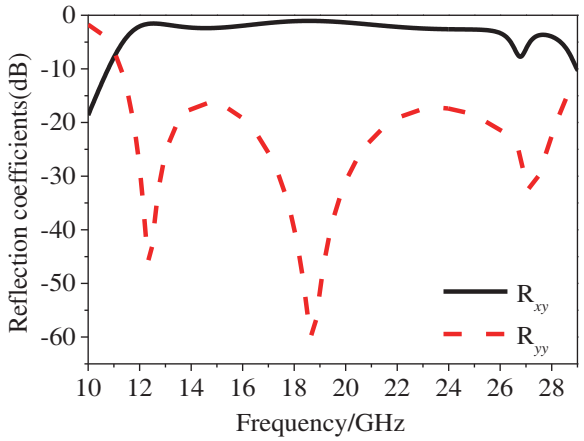

FIGURE 2. Co- and cross-polarization transmission coefficients of the unit cell.

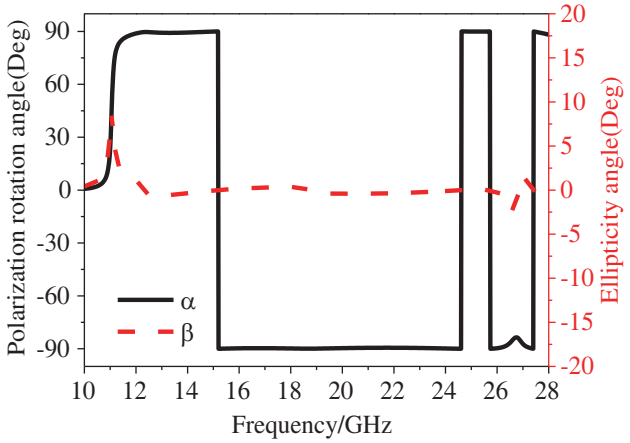

FIGURE 3. Polarization rotation angle α and elliptic angle β varying with frequency.

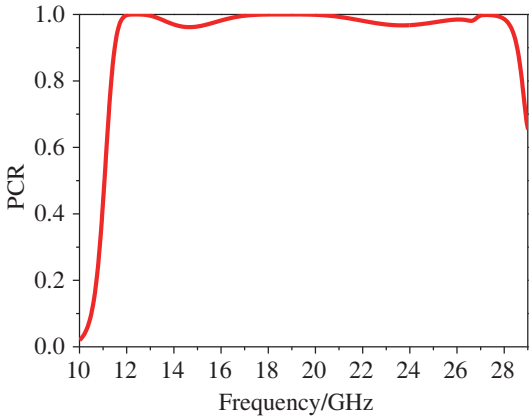

FIGURE 4. PCR of the unit cell varying with frequency.

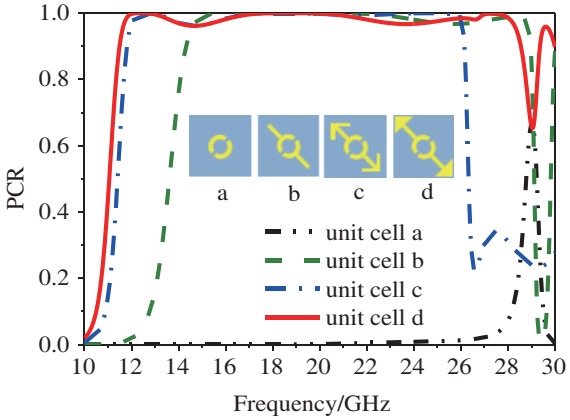

FIGURE 5. Evolution of the proposed unit cells and their corresponding PCRs.

$$S_3 = 2T_{yy}T_{xy}\sin\delta \tag{9}$$

The calculated results are plotted in Fig. 3. At frequencies of 11.5–28.5 GHz, α is close to 90°, and β is close to 0°, indicating that the proposed BASR polarization converter achieves a near perfect linear cross-polarization transition.

Without loss of generality, the polarization conversion ratio (PCR) is calculated here to describe the conversion efficiency:

$$\text{PCR} = \frac{R_{xy}^2}{R_{xy}^2 + R_{yy}^2} \tag{10}$$

The PCR when a y-polarized wave is incident normally is plotted in Fig. 4. It is noted that PCR is greater than 90% in the frequency range of 11.5–28.5 GHz, and it reaches 100% at three resonant frequencies of 12.4, 18.7, and 27.1 GHz. This indicates that almost all the energy of the y-polarized incident wave is converted into x-polarized reflection. As the unit cell is diagonally symmetrical, similar performance would be displayed for x-polarized incident wave.

2.2. Analysis of the Polarization Conversion Principle

In order to clarify the mechanism, the evolution of the unit cell and its corresponding PCR are described below, as shown in Fig. 5. One can see that the split ring pair generates an operation point at 28.6 GHz with PCR lower than 0.7. To promote the performance, two narrow strips are added along the 45° direction, which produces new resonance, and then a broad band from 14.3 to 28.9 GHz with PCR higher than 0.9 is achieved. Then, to cover the Ku-band, a pair of right-angled arrows are introduced, and resonance at 12.4 GHz is generated. As a result, the operation band shifts down to 11.7–26.2 GHz. To cover the K-band, the right-angled arrows are replaced by right-angled triangles forming a pair of bow-and-arrow shaped split rings. The triangles, together with the split rings, produces a new resonance at 27.1 GHz. Finally, due to the multiple resonances, the polarization converter achieves a PCR of over 90% in the ultra-wide frequency band of 11.5–28.5 GHz, covering the entire Ku and K bands.

To intuitively interpret the physical mechanism of the PCM, surface current distributions at the three resonant frequencies of 12.4, 18.7, and 27.1 GHz are illustrated in Fig. 6. Y-polarized

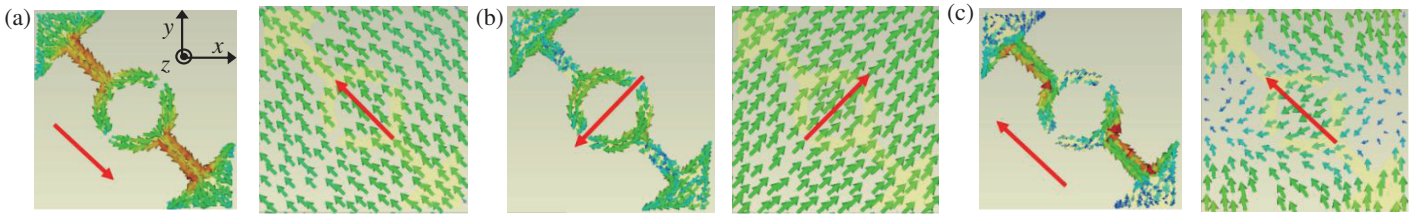

FIGURE 6. Surface current distributed at the BASR and the grounded plane at: (a) 12.4 GHz (b) 18.7 GHz (c) 27.1 GHz.

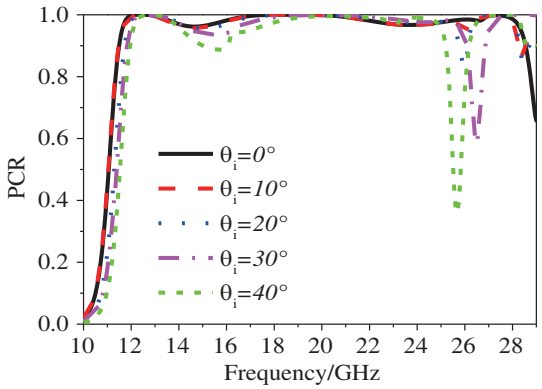

FIGURE 7. PCR for different incident angles.

wave is normally incident in simulation. The red arrows indicate the direction of the resultant current on the BASR and the grounded plane. As illustrated in Fig. 6, at 12.4 GHz, the top surface currents mainly concentrate in the narrow strips, and they are opposed to the currents generated on the grounded plane, generating equivalent magnetic resonance. Similarly, at 18.7 GHz, the polarization converter also generates equivalent magnetic resonance. At 27.1 GHz, the currents concentrate in the edge of the split ring, narrow strips, and triangles. They are parallel to the current at ground plane, producing an equivalent electrical resonance [3]. Thus, multiple electromagnetic resonances together give rise to an ultrawide polarization conversion bandwidth.

2.3. Angular Stability

Angular stability refers to the sable conversion performance of the polarization converter when the incident angle increases. To explore the applicability of the PCM in RCS reduction of curved surfaces, the angular stability needs to be discussed. Fig. 7 describes the PCR varying with frequency for y-polarized waves at different incident angles. It is noted that the PCR and polarization conversion bandwidth are stable when the incidence angles vary from $0°$ to $\pm 40°$. At angles of $30°$ and $40°$, PCR remains greater than 0.8 with small bandwidth loss (1.25% and 1.65%, respectively). The main reason is that larger incidence angle will increase the propagation phase of the EM wave, and then, the destructive interference degrades its performance [31].

3. APPLICATION OF PCM TO RCS REDUCTION

Based on the principle of phase cancellation [32], the PCM and its mirror unit cells can be laid out in a checkerboard array to realize RCS reduction. Fig. 8 depicts the PCM and its mirror unit cells, and the cross-polarization reflection phase difference between them. One can observe that a $180°$ phase difference in the ultra-wideband is obtained. Therefore, they are suitable for the application of RCS reduction.

3.1. RCS Reduction of Planar Surface

To realize RCS reduction, a checkerboard array is designed as mentioned above, which consists of PCM and their mirror cells laid out in four quadrants. Each quadrant is composed of 5×5 cells, as depicted in Fig. 9. The overall size is $60 \times 60 \times 1.6$ mm^3 ($2.28\lambda \times 2.28\lambda \times 0.06\lambda$, λ is the operating wavelength at the lowest operating frequency). With the tessellated array arrangement, phase shifts of $+90°$ and $-90°$ to the cross-polarized reflected wave will be generated by the PCM and its mirror units, which cancel out each other and lead to RCS reduction in the incoming wave.

Figure 10 gives the comparison the monostatic RCS of the proposed checkerboard array with that of a copper sheet with the same dimension under y-polarized normal incidence. It is indicated that the PCMs obtain a consistent 7 dB RCS reduction at 11.4–29.6 GHz. The maximum RCS reductions are -26 dB, -25 dB, and -30 dB at 11.9, 19.1, and 26.9 GHz, respectively. Additionally, at frequencies of 11.6–13.3 GHz, 16.8–22.4 GHz, and 25.5–29 GHz, the RCS reduction is larger than 10 dB.

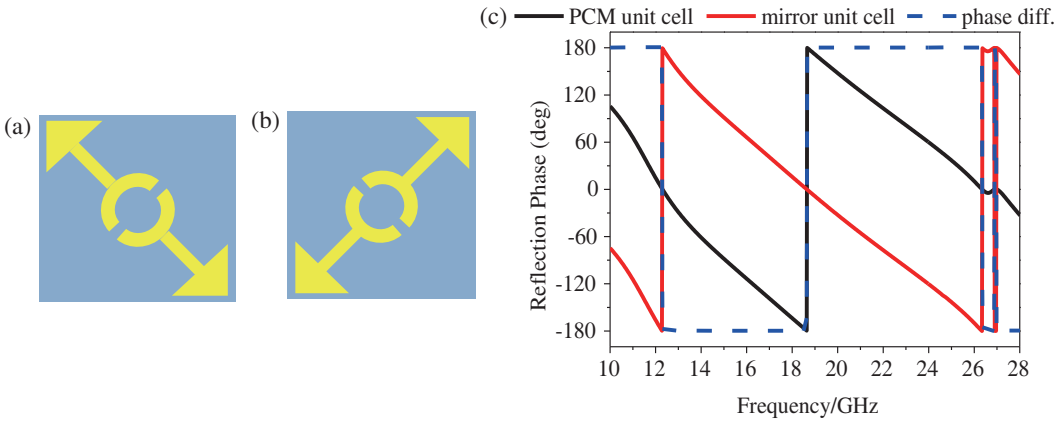

FIGURE 8. (a) The proposed PCM and (b) its mirror unit cells, and (c) the cross-polarization reflection phase of the unit cells, and the phase difference between them.

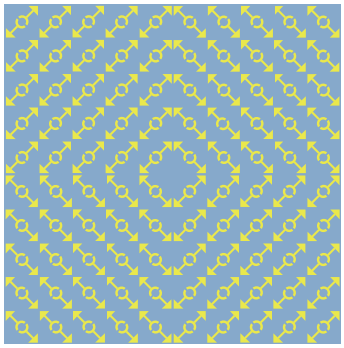

FIGURE 9. Checkerboard array.

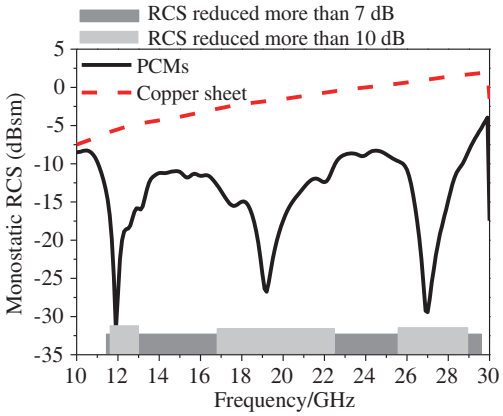

FIGURE 10. The simulated RCS of the PCMs array and the copper sheet.

3.2. RCS Reduction of Curved Surfaces

For the application of curved surfaces, the PCMs are conformal onto cylindrical surfaces with different curvature radii. Also, copper sheets of the same size are conformal to the same surfaces for comparing.

Figure 11(a) plots the schematic diagram of central angle α. Figs. 11(b)–(d) display the simulated RCS of the checkerboard array and copper sheet when the central angle α of cylindrical surfaces are 30°, 60°, and 90°. One can see that the RCS reduction is still substantial. The maximum reductions are 34.8, 23.5, and 23.9 dB for 30°, 60°, and 90° central angle, respectively. Additionally, Fig. 12 depicts the 3D scattering patterns for y-polarized waves normal incident to planar and conformal curved PCMs at 18.7 GHz. The reflected energy is dispersed in the non-incident direction. The main reason is the phase cancellation of the reflected waves. As previously mentioned, the proposed polarization converter can maintain a stable bandwidth and PCR at wide incidence angles. Thus, the 180° phase difference is still maintained when the checkerboard surface is conformal onto cylindrical surfaces.

4. MEASUREMENT AND PERFORMANCE COMPARISON

To validate the performance of the proposed polarization converter, a prototype composed of 16 × 16 cells has been fabricated and measured, as illustrated in Fig. 13. During measurement, the polarization converter is surrounded by absorbing material. Two horn antennas are placed in front of the polarization converter as transmitter and receiver. The network vector analyzer N5230A was used to measure the reflection coefficient. Both antennas are placed vertically to obtain the co-polarization reflection coefficient, and the receiving antenna is rotated by 90° to obtain the cross-polarization reflection coefficient. To measure the oblique incidence performance, an angle measuring device and a metal reflector plane are used, as illustrated in Figs. 13(b) and (c). The sample and metal reflector are rotated together by the same angle while the horn antennas keep still.

Figure 14 plots the simulated and experimental results of the reflection coefficient. As shown, the measured results agree well with the simulated ones. Slight frequency shift is observed at high frequencies for R_{xy} at different incident angles. The limited number of cell repetitions, processing and measuring errors accumulate together to form the total error.

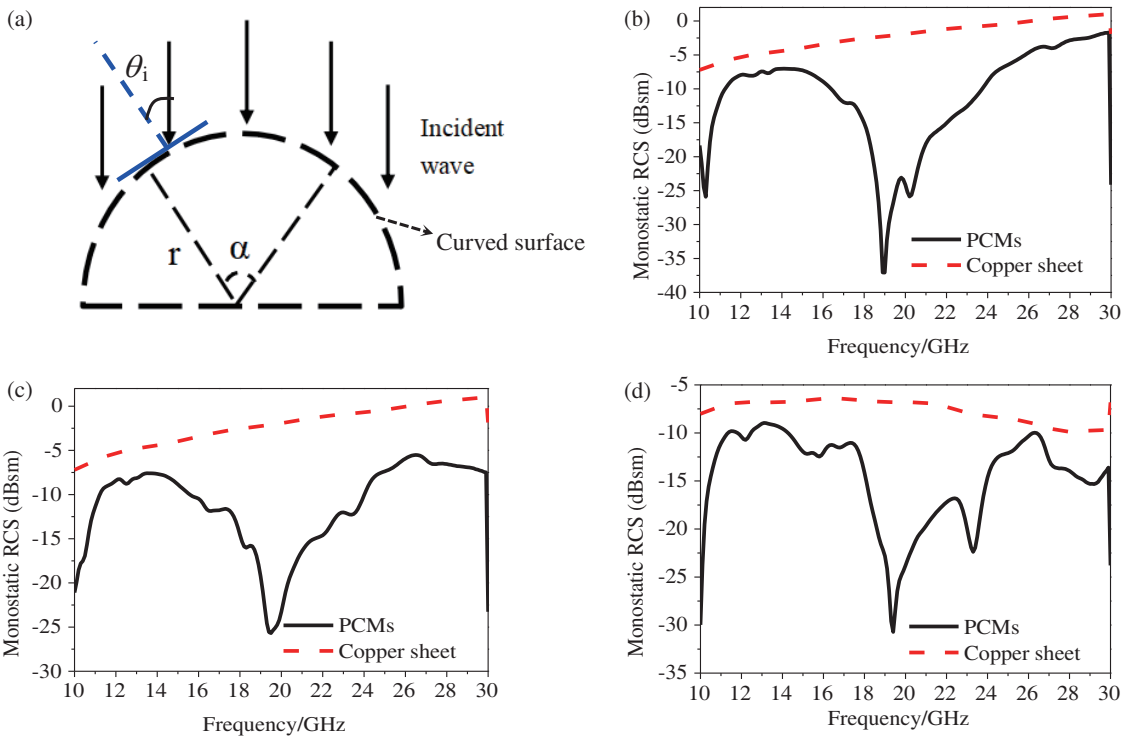

FIGURE 11. Simulated RCS of PCMs and copper sheet conformal at different central angles: (a) $\alpha = 30^\circ$ (b) $\alpha = 60^\circ$ (c) $\alpha = 90^\circ$.

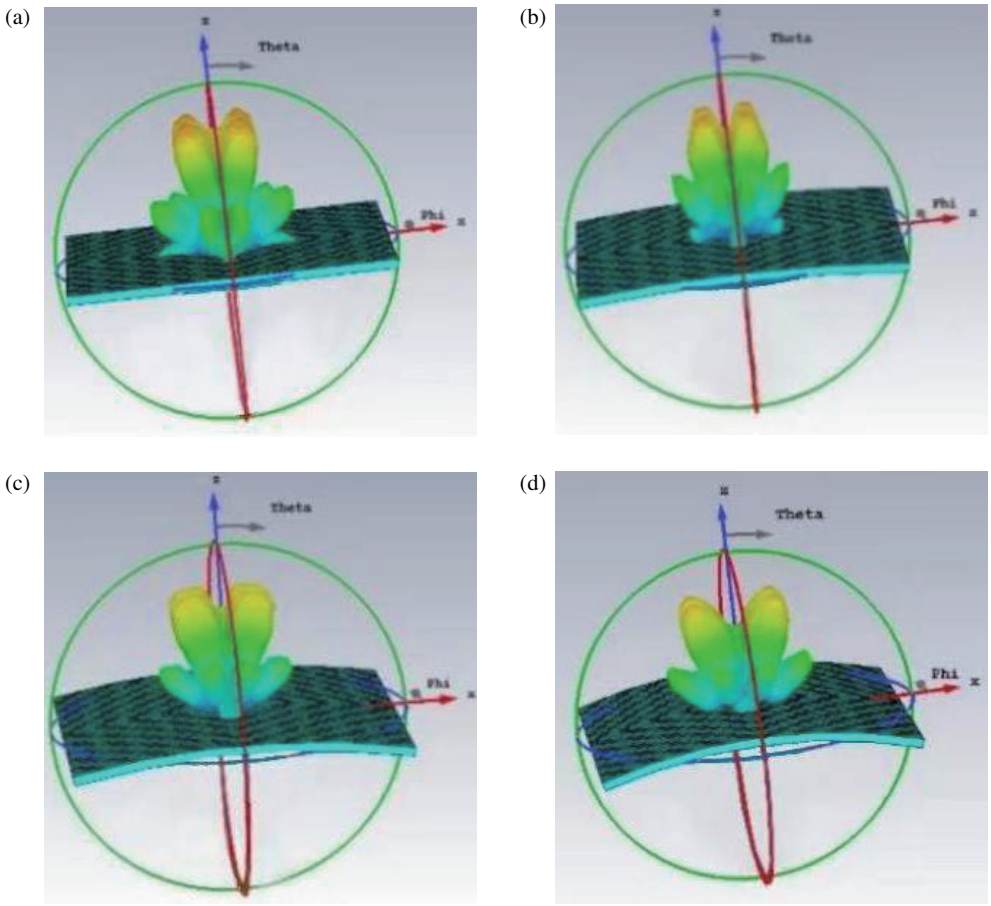

FIGURE 12. Simulated 3-D scattering patterns of PCMs at different central angles at 18.7 GHz: (a) $\alpha = 0$, (b) $\alpha = 30^\circ$, (c) $\alpha = 60^\circ$, (d) $\alpha = 90^\circ$.

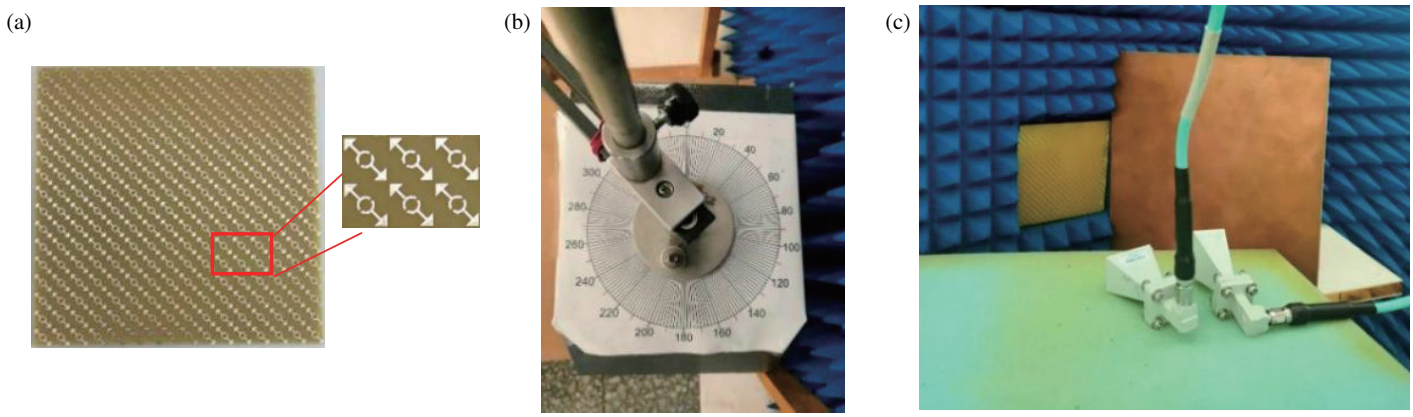

FIGURE 13. Photographs of: (a) the sample. (b) Angle measuring apparatus, and (c) Measuring environment.

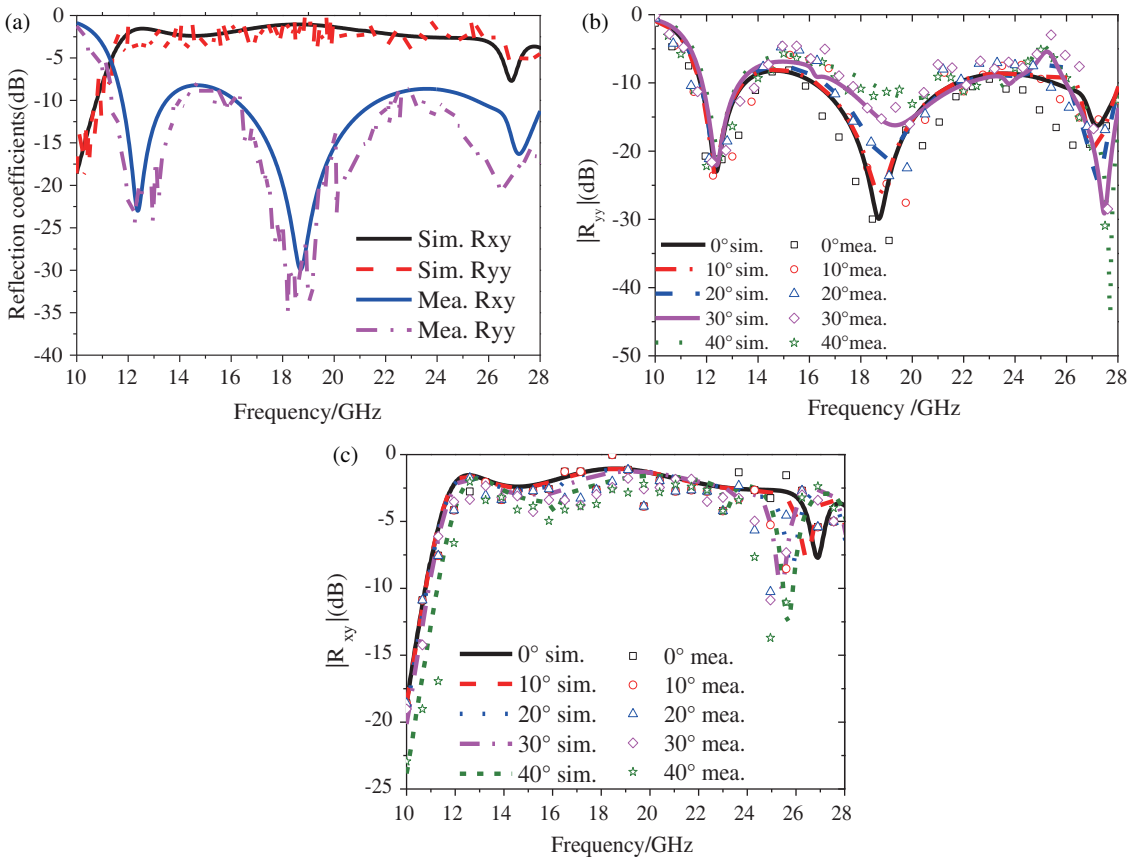

FIGURE 14. Simulated and measured (a) reflection coefficients, (b) $|R_{yy}|$ and $|R_{xy}|$ for different θ.

Performance of the proposed PCM is compared with that in other literatures in Table 2. It is noted that the PCMs in [28, 34] are not suitable for wide angle incidence. In [1, 30, 35], the application in RCS reduction was not discussed. Additionally, the PCR in [1] is low, and the polarization conversion bandwidth in [30] is narrow. The incidence angle in [35] is slightly wider than that of this work; however, the operation band is narrower. In [3, 33], the performance of PCM and application in RCS reduction of both plane and curved surfaces were explored comprehensively. The incidence angle in [33] is wider than that of this work, while the bandwidth of polarization conversion and RCS reduction is small. Compared with the PCM with sandwiched air layer in [3], this work has lower profile, wider incidence angle, higher PCR, lower cost, and lower fabrication complexity. In a word, excellent comprehensive performance is achieved using a low cost and simple processing structure in this paper.

TABLE 2. Performance comparison with reported PCMs.

Refs.	U.C. size (mm^3)	PCM S.M.	P.C.B. (GHz)	PCR	I.A.	B.W. for P.S (GHz)	B.W. for C.S (GHz)	cost
[1]	$7 \times 7 \times 2.4$	FR-4	5.3–10.8	60%	$\pm 45^\circ$	None	No	Low
[3]	$7 \times 7 \times 4$ $(0.15\lambda \times 0.15\lambda \times 0.08\lambda)$	Rogers RT/duroid 5880	6.3–20.5 (106%)	$> 80\%$	$\pm 35^\circ$	5.5–20.5 (115%)	10.1–15.4, (42%)	High
[28]	$6.5 \times 6.5 \times 2.1$ $(0.25\lambda \times 0.25\lambda \times 0.08\lambda)$	Rogers RT 5880	11.5–34.5 (100%)	$> 90\%$	None	10.9–13.1 15.7–19.0 27.5–33.0 (55.5%)	None	High
[30]	$8 \times 8 \times 0.8$ $(0.24\lambda \times 0.24\lambda \times 0.02\lambda)$	Rogers RT 5880	8.8	95%	$\pm 30^\circ$	None	None	High
[33]	$3.6 \times 3.6 \times 0.15$ $(0.38\lambda \times 0.38\lambda \times 0.016\lambda)$	polyimide (PI)	31.4–32.6 (2.5%)	$> 90\%$	$\pm 45^\circ$	32 GHz	32 GHz	High
[34]	$8.1 \times 8.1 \times 3.1$ $(0.18\lambda \times 0.18\lambda \times 0.07\lambda)$	FR-4	6.53–12.07 (59.6%)	$> 88\%$	None	None	None	Low
[35]	$5 \times 5 \times 2.12$ $(0.19\lambda \times 0.19\lambda \times 0.08\lambda)$	PET&PVC	11.3–20.2 (56.5%)	$> 85\%$	$\pm 45^\circ$	None	None	Low
This work	$6 \times 6 \times 1.6$ $(0.23\lambda \times 0.23\lambda \times 0.06\lambda)$	FR-4	11.5–28.5 (85%)	$> 90\%$	$\pm 40^\circ$	11.6–13.3, 16.8–22.4, 25.5–29 (55.1%)	18.2–23.7 (26.3%)	Low

(U.C. size: Unit cell size; PCM S.M.: PCM substrate material; P.C.B.: Polarization conversion bandwidth; I.A.: Incident angle; B.W. for P.S.:10 dB RCS reduction bandwidth for planar surface. B.W. for C.S.: 10 dB RCS reduction bandwidth for curved surface with 90° central angle.)

5. CONCLUSION

This paper presents a novel linear cross-polarization converter. The overall dimension of the BASR PCM unit cell is $0.23\lambda \times 0.23\lambda \times 0.06\lambda$, and the processing can be achieved using only traditional printed circuit board process. The PCR of more than 90% over an ultra-wideband of 11.5–28.5 GHz is obtained by introducing multiple resonances. Also, the angular stability is discussed and measured, and PCR of higher than 0.8 over an incidence angle of 0°–40° is realized. In addition, the PCM cell has a phase difference of 180° with its mirror cell, allowing it to be applied to reduce RCS for both planar and curved surfaces. 10 dB RCS reduction with relative bandwidth of 55.1% for planar surfaces and 26.3% for curved surfaces with 90° central angle are realized. The proposed surface has excellent comprehensive performance including high PCR, wide incidence angle, low thickness, simple processing, and low cost, which make it a promising candidate for both general and stealth applications in Ku- and K-bands.

ACKNOWLEDGEMENT

This research work was funded by the National Natural Science Foundation of China (62071282) and the Fundamental Research Program of Shanxi Province (202203021211295).

REFERENCES

[1] Khan, M. I., Q. Fraz, and F. A. Tahir, "Ultra-wideband cross polarization conversion metasurface insensitive to incidence angle," *Journal of Applied Physics*, Vol. 121, No. 4, 045103, Jan. 2017.

[2] Sun, W., Q. He, J. Hao, and L. Zhou, "A transparent metamaterial to manipulate electromagnetic wave polarizations," *Optics Letters*, Vol. 36, No. 6, 927–929, 2011.

[3] Chatterjee, J., A. Mohan, and V. Dixit, "Ultrawideband RCS reduction of planar and conformal surfaces using ultrathin polarization conversion metasurface," *IEEE Access*, Vol. 10, 36 563–36 575, 2022.

[4] Zhang, J., L. Yang, L. Li, T. Zhang, H. Li, Q. Wang, Y. Hao, M. Lei, and K. Bi, "High-efficiency polarization conversion phase gradient metasurface for wideband anomalous reflection," *Journal of Applied Physics*, Vol. 122, No. 1, 2017.

[5] Zhu, X.-C., W. Hong, K. Wu, H.-J. Tang, Z.-C. Hao, J.-X. Chen, H.-X. Zhou, and H. Zhou, "Design of a bandwidth-enhanced polarization rotating frequency selective surface," *IEEE Transactions on Antennas and Propagation*, Vol. 62, No. 2, 940–944, Feb. 2014.

[6] Du, X., H. Lin, X. Shi, Y. Mao, and Y. Wu, "Triple-band metamaterial polarization converter based on substrate integrated waveguide technology," in *Cross Strait Radio Science & Wireless Technology Conference*, 1–3, 2020.

[7] Sohail, I., Y. Ranga, K. P. Esselle, and S. G. Hay, "A linear to circular polarization converter based on jerusalem-cross fre-

quency selective surface," in *2013 7th European Conference on Antennas and Propagation (EUCAP)*, 2141–2143, Gothenburg, Sweden, Apr. 2013.

[8] Li, L., Y. Li, Z. Wu, F. Huo, Y. Zhang, and C. Zhao, "Novel polarization-reconfigurable converter based on multilayer frequency-selective surfaces," *Proceedings of The IEEE*, Vol. 103, No. 7, 1057–1070, 2015.

[9] Kundu, D., A. Mohan, A. Chakrabarty, J. Singh, and D. Singh, "An ultrathin linear-to-circular polarization converter with wide axial ratio bandwidth," in *Proceedings of The 2019 IEEE Asia-pacific Microwave Conference (APMC)*, 929–931, Singapore, Dec. 2019.

[10] Li, Z., J. Su, and Z. Li, "Design of polarization converter based on the high efficiency transmission phase gradient metasurface," in *2017 IEEE Sixth Asia-pacific Conference on Antennas and Propagation (APCAP)*, 1–3, Xian, China, Oct. 2017.

[11] Peng, L., X.-F. Li, X. Jiang, and S.-M. Li, "A novel THz half-wave polarization converter for cross-polarization conversions of both linear and circular polarizations and polarization conversion ratio regulating by graphene," *Journal of Lightwave Technology*, Vol. 36, No. 19, 4250–4258, Oct. 2018.

[12] Khajeh, A., Z. Hamzavi-Zarghani, and A. Yahaghi, "Design and simulation of a polarization converter based on graphene metasurfaces," in *2020 28th Iranian Conference on Electrical Engineering (ICEE)*, 1473–1476, Univ Tabriz, Fac Elect & Comp Engn, Aug. 2020.

[13] Bakhtiari, B. and H. Oraizi, "Tunable terahertz polarization converter based on graphene metasurfaces," in *2020 14th European Conference on Antennas and Propagation (EUCAP 2020)*, 1–4, Copenhagen, Denmark, Mar. 2020.

[14] Yang, W. L. and X. Gao, "A reconfigurable polarization converter based on active metasurface," in *2018 Cross Strait Quad-regional Radio Science and Wireless Technology Conference (CSQRWC)*, 1–2, Xuzhou, China, Jul. 2018.

[15] Zhou, Q., G. Du, and D. Wang, "Ultra-broadband linear polarization converter based on single-layer reflective metasurface," in *2020 IEEE Mtt-s International Conference on Numerical Electromagnetic and Multiphysics Modeling and Optimization (NEMO 2020)*, 1–4, Hangzhou, China, Dec. 2020.

[16] Lin, B., L. Lv, J. Guo, Z. Liu, X. Ji, and J. Wu, "An ultra-wideband reflective linear-to-circular polarization converter based on anisotropic metasurface," *IEEE Access*, Vol. 8, 82 732–82 740, 2020.

[17] Fu, C., Z. Sun, L. Han, and C. Liu, "Dual-bandwidth linear polarization converter based on anisotropic metasurface," *IEEE Photonics Journal*, Vol. 12, No. 2, 1–11, Apr. 2020.

[18] Wang, L., Y. Jiang, J. Wang, W. Cao, X. Gao, and X. Yu, "Ultra-broadband reconfigurable linear-to-circular polarization converter based on metasurface in terahertz frequency," in *2017 IEEE Sixth Asia-pacific Conference on Antennas and Propagation (APCAP)*, 1–3, Xian, China, Oct. 2017.

[19] Khan, S. and T. F. Eibert, "A dual-band metasheet for asymmetric microwave transmission with polarization conversion," *IEEE Access*, Vol. 7, 98 045–98 052, 2019.

[20] Wang, S.-Y., J.-D. Bi, W. Liu, W. Geyi, and S. Gao, "Polarization-insensitive cross-polarization converter," *IEEE Transactions on Antennas and Propagation*, Vol. 69, No. 8, 4670–4680, Aug. 2021.

[21] Gao, X., X. Han, W.-P. Cao, H. O. Li, H. F. Ma, and T. J. Cui, "Ultrawideband and high-effificiency linear polarization converter based on double V-shaped metasurface," *IEEE Transactions on Antennas and Propagation*, Vol. 63, No. 8, 3522–3530, 2015.

[22] Yu, H. and J. Su, "Dual-band and high-efficiency reflective polarization converter based on strip grating," in *2020 IEEE International Symposium on Antennas and Propagation and North American Radio Science Meeting*, 967–968, Electr Network, Jul. 2020.

[23] Izhar, R., M. E. Mustafa, M. S. Wahidi, and F. A. Tahir, "An anisotropic dual-broadband reflective polarization converter metasurface," in *IEEE International Conference on Computational Electromagnetics*, 1–2, 2019.

[24] Khan, M. I., Q. Fraz, and F. A. Tahir, "Ultra-wideband cross polarization conversion metasurface insensitive to incidence angle," *Journal of Applied Physics*, Vol. 121, No. 4, Jan. 2017.

[25] Pandit, S., A. Mohan, and P. Ray, "Low-RCS low-profile four-element mimo antenna using polarization conversion metasurface," *IEEE Antennas and Wireless Propagation Letters*, Vol. 19, No. 12, 2102–2106, Dec. 2020.

[26] Ren, Z., Y.-Q. Liu, Y. Wang, L. Lu, K. Qi, and H. Yin, "Ultra-broadband RCS reduction based on optimized coding "whale-shaped" polarization conversion metasurface with angular stability," *IEEE Access*, Vol. 10, 50 479–50 486, 2022.

[27] Liu, J., J.-Y. Li, and Z. N. Chen, "Broadband polarization conversion metasurface for antenna RCS reduction," *IEEE Transactions on Antennas and Propagation*, Vol. 70, No. 5, 3834–3839, May 2022.

[28] Hong, T., S. Wang, Z. Liu, and S. Gong, "RCS reduction and gain enhancement for the circularly polarized array by polarization conversion metasurface coating," *IEEE Antennas and Wireless Propagation Letters*, Vol. 18, No. 1, 167–171, Jan. 2019.

[29] Jing, X., X. Gui, P. Zhou, and Z. Hong, "Physical explanation of fabry-pérot cavity for broadband bilayer metamaterials polarization converter," *Journal of Lightwave Technology*, Vol. 36, No. 12, 2322–2327, Jun. 2018.

[30] Baghel, A. K., S. S. Kulkarni, and S. K. Nayak, "Linear-to-cross-polarization transmission converter using ultrathin and smaller periodicity metasurface," *IEEE Antennas and Wireless Propagation Letters*, Vol. 18, No. 7, 1433–1437, Jul. 2019.

[31] Lei, Z. and T. Yang, "Converting state of polarization with a miniaturized metasurface device," *IEEE Photonics Technology Letters*, Vol. 29, No. 7, 615–618, Apr. 2017.

[32] Chen, W., C. A. Balanis, C. R. Birtcher, and A. Y. Modi, "Cylindrically curved checkerboard surfaces for radar cross-section reduction," *IEEE Antennas and Wireless Propagation Letters*, Vol. 17, No. 2, 343–346, Feb. 2018.

[33] Wang, Y., F. Qi, Z. Liu, P. Liu, and W. Li, "Ultrathin and flexible reflective polarization converter based on metasurfaces with overlapped arrays," *IEEE Antennas and Wireless Propagation Letters*, Vol. 19, No. 12, 2512–2516, Dec. 2020.

[34] Zheng, Q., C. Guo, and J. Ding, "Wideband metasurface-based reflective polarization converter for linear-to-linear and linear-to-circular polarization conversion," *IEEE Antennas and Wireless Propagation Letters*, Vol. 17, No. 8, 1459–1463, Aug. 2018.

[35] Wang, Q., X. Kong, X. Yan, Y. Xu, S. Liu, J. Mo, and X. Liu, "Flexible broadband polarization converter based on metasurface at microwave band," *Chinese Physics B*, Vol. 28, No. 7, 074205, 2019.